The Journal of Eukaryotic Microbiology

ISOP Published by the International Society of Protistologists

Journal of Eukaryotic Microbiology ISSN 1066-5234

ORIGINAL ARTICLE

An Integrative Investigation of *Parabistichella variabilis* (Protista, Ciliophora, Hypotrichia) Including Its General Morphology, Ultrastructure, Ontogenesis, and Molecular Phylogeny

Jingyi Dong[a,b,1], Xumiao Chen[c,1], Yongqiang Liu[a], Bing Ni[b], Xinpeng Fan[b], Lifang Li[d] & Alan Warren[e]

a Institute of Evolution & Marine Biodiversity, and College of Fisheries, Ocean University of China, Qingdao 266003, China
b School of Life Sciences, East China Normal University, Shanghai 200241, China
c Department of Marine Organism Taxonomy and Phylogeny, Institute of Oceanology, Chinese Academy of Sciences, Qingdao 266071, China
d Marine College, Shandong University, Weihai 264209, China
e Department of Life Sciences, Natural History Museum, London SW7 5BD, United Kingdom

Keywords
Buccal seal; contractile vacuole pore; extrusomes; pharyngeal disks; taxonomic assignment.

Correspondence
X. Fan, School of Life Sciences, East China Normal University, Shanghai 200241, China
e-mail: xpfan@bio.ecnu.edu.cn
Telephone number: +86-21-54345473
Fax number: +86-21-54341006
L. Li, Marine College, Shandong University, Weihai 264209, China
e-mail: qd_liliy@sina.com
Telephone number: +86-0631-5688303
Fax number: +86-0631-5688303

Received: 27 September 2019; revised 30 April 2020; accepted May 14, 2020.
Early View publication June 15, 2020

doi:10.1111/jeu.12809

[1]Both authors contributed equally.

ABSTRACT

Hypotrichs are a highly differentiated and very diverse group of ciliated protists. Their systematics and taxonomy are challenging and call for detailed investigations on their general morphology, ultrastructure, ontogenesis, and molecular phylogeny. Here, a comprehensive study is conducted on a brackish water population of *Parabistichella variabilis* using light and electron microscopy and phylogenetic analyses based on small subunit ribosomal DNA sequence data. Its morphology, including the infraciliature, pellicle, nuclei, buccal seal, and extrusomes, is documented. The present findings indicate that in *P. variabilis*: (i) the cortical granules are extrusomes, which differ from those of other hypotrichs; (ii) the buccal seal is bounded by the plasma membrane and contains a single layer of longitudinal microtubules; (iii) two contractile vacuoles might be present rather than one; and (iv) the pharyngeal disks are bounded by a single membrane. Early-to-middle stages of ontogenesis are described for the first time, enabling the complete characterization of this process. Phylogenetic analyses indicate that *Parabistichella variabilis* is closely related to several species from different genera, such as *Orthoamphisiella breviseries*, *Uroleptoides magnigranulosus*, and *Tachysoma pellionellum*. However, ultrastructural and gene sequence data for more taxa are needed in order to resolve the systematics of *Parabistichella*.

CILIATES in the subclass Hypotrichia Stein, 1859, exhibit extremely diverse morphological and ontogenic features. This group includes numerous taxa with uncertain systematic positions, mainly as a result of insufficient descriptions of their morphology and the lack of ontogenic and molecular data (Berger 1999, 2006, 2008, 2011; Paiva et al. 2012; Park et al. 2013; Schmidt et al. 2007; Song and Shao 2017; Wang et al. 2019).

The genus *Parabistichella* was established by Jiang et al. (2013). It was treated as incertae sedis in Hypotrichia because its general morphology and ontogenesis show similarities with both the bakuellids and amphisiellids. For example, the possession of three frontal cirri, a midventral complex composed of cirral pairs and row(s), and seven or more frontoventral-transverse streaks during cell division suggest that it is a "bakuellid-like" hypotrich (Berger 2006). However, the possession of a frontoventral row composed of at least two parts, similar to the amphisiellid median cirral row, is typical of amphisiellids (Berger 2008). Foissner (2016) described one species (with two subspecies) of *Parabistichella* and transferred four species previously assigned to the genus *Bistichella*, and one species formerly affiliated with the genus *Keronopsis*, to *Parabistichella*. He also provided an

improved diagnosis of the genus as follows: (i) two or three short frontal cirral rows [referred to here and by Jiang et al. (2013), as midventral pairs] and two or three long frontoventral cirral rows [both here and in Jiang et al. (2013), these are referred to as the frontoventral and midventral cirral rows]; (ii) three or four enlarged frontal cirri; (iii) one or more buccal cirri; (iv) transverse cirri present; (v) single left and right marginal rows; (vi) dorsal kinety pattern of the *Gonostomum*-type (Foissner 2016).

The type species of *Parabistichella*, *P. variabilis,* was described by Jiang et al. (2013) in terms of its general morphology, middle-to-late stages of ontogenesis, and physiological regeneration. Ultrastructural data and descriptions of the early ontogenetic stages were, however, lacking. The main aims of the present study are to provide further data on the morphology (including the ultrastructure), ontogenesis, and molecular phylogeny of *P. variabilis*. The classification and phylogeny of the genus *Parabistichella* are also discussed.

MATERIALS AND METHODS

Sampling and cultivation

Samples containing *Parabistichella variabilis* were collected from surface sediments of a marsh wetland at North Beach (31°52′2.21″N 121°18′32.31″E), Chongming Island, Shanghai, southeastern China, on 14 November 2015. The water salinity was 10 PSU, and the temperature was 25 °C. Approximately ten cells were isolated and transferred to Petri dishes to set up a raw culture at 26 °C using artificial brackish water (10 PSU) prepared with Golden Trump sea salt. Wheat grains were added to foster the growth of bacteria and scuticociliates as a food source. Specimens from the raw culture were used for all subsequent studies.

Light microscopy

Isolated specimens were observed in vivo, using bright field and differential interference contrast microscopy. The infraciliature was revealed by the protargol silver staining method (Wilbert 1975). The protargol powder was prepared according to Pan et al. (2013). Counts and measurements of protargol-stained specimens were performed at 1,000X magnification.

Deposition of voucher material

Five voucher slides with protargol-stained specimens of *Parabistichella variabilis* have been deposited in the collection of the Laboratory of Protozoology, Ocean University of China, Qingdao, China (registration numbers: DJY2015111405-01, -02, -03, -04, 05).

Scanning electron microscopy (SEM)

Individuals for SEM were treated mainly according to the method described by Gu and Ni (1993). Cells in about 1.5 ml of culture medium were fixed in a 1:6 mixture of 1% OsO_4 and a saturated solution of $HgCl_2$ at room temperature (about 25 °C) for 10 min and rinsed with 0.2 M cacodylate buffer. The fixed cells were dehydrated in a graded series of ethanol for about 8 min at each concentration, dried in a critical point dryer (Leica EM CPD300), and coated with platinum by a sputter coater (Leica EM ACE600). A scanning electron microscope (Hitachi S-4800) was used to study the specimens at an accelerating voltage of 10 kV.

Transmission electron microscopy (TEM)

Specimens were prepared for TEM according to the procedure of Gu et al. (2002) and Gu and Ni (1995). The cells (in about 700 μl culture medium) were fixed in a mixture of 100 μl of 2% OsO_4 and 600 μl of 2.5% glutaraldehyde at 4 °C for 10 min followed by 300 μl of 2% OsO_4 in 0.2 M cacodylate buffer at 4 °C for 60 min. The fixed cells were dehydrated in a graded acetone series and then embedded with Eponate 12 resin. Ultrathin sections (about 70 nm) were stained with uranyl acetate and lead citrate and investigated with a transmission electron microscope (Hitachi HT7700) at an accelerating voltage of 220 kV.

DNA extraction, PCR amplification, gene sequencing, and phylogenetic analyses

Several cells were isolated and washed five times with sterilized water (0.22 μm filtered) to remove potential contamination. The total genomic DNA was extracted using the DNeasy Blood and Tissue Kit (Qiagen, Valencia, CA) according to the methods described by Gao et al. (2016). Q5 Hot Start High-Fidelity DNA Polymerase (Cat. #M0493 L, New England Biolabs, Ipswich, MA, USA) was used to amplify the small subunit (SSU) rDNA with the primers 18S-F (5′-AAC CTG GTT GAT CCT GCC AGT-3′) and 18S-R (5′-TGA TCC TTC TGC AGG TTC ACC TAC-3′) designed by Medlin et al. (1988). The conditions for polymerase chain reaction (PCR) amplification were according to Huang et al. (2016).

In addition to the new consensus sequence, 95 SSU rDNA sequences downloaded from GenBank were used in the phylogenetic analyses. The GenBank accession numbers of the 20 core urostylids are as follows: *Bakuella* sp. KC631826, *Bakuella incheonensis* KR024011, *Diaxonella pseudorubra* GU942564, *Bakuella litoralis* KR024010, *Neobakuella flava* GU967698, *Apobakuella fusca* JN 008942, *Bakuella granulifera* KJ958489, *Urostyla grandis* HM140388, *Metaurostylopsis struederkypkeae* JQ424832, *Metaurostylopsis salina* EU220229, *Metaurostylopsis cheni* GU170204, *Metaurostylopsis antarctica* JF906730, *Anteholosticha randani* KU234524, *Trichototaxis marina* KJ845346, *Antiokeronopsis flava* KF806444, *Uroleptopsis citrina* FJ870094, *Metaurostylopsis sinica* JQ955541, *Apoholosticha sinica* KJ000285, *Heterokeronopsis pulchra* JQ083600, and *Nothoholosticha fasciola* FJ377548. For the GenBank accession numbers of the other

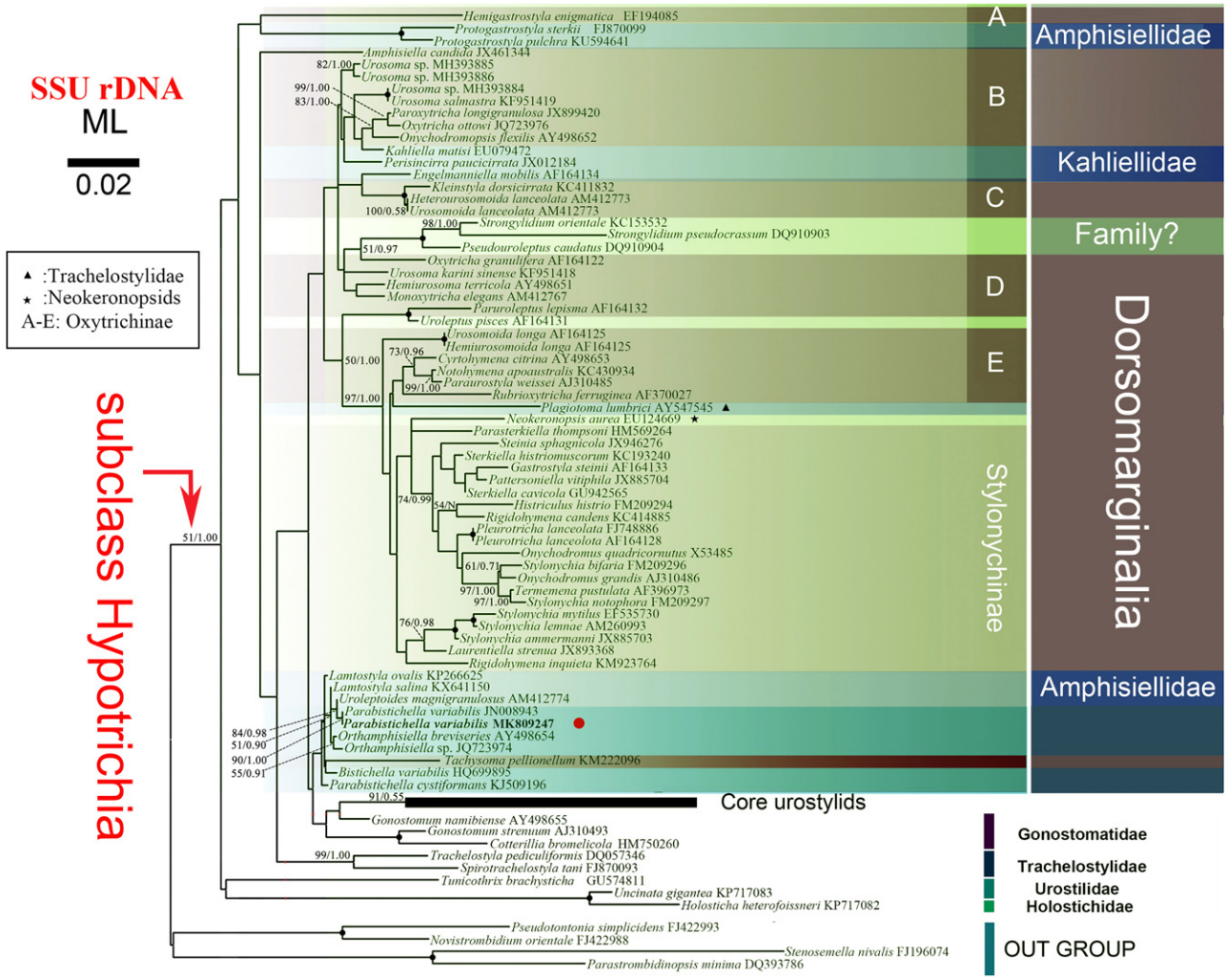

Figure 1 Maximum likelihood (ML) tree inferred from SSU rDNA sequences showing representative taxa and the newly sequenced species (bold font). Bootstrap values above 50 for ML and posterior probability values above 0.50 for Bayesian inference (BI) are given beside nodes. "N" indicates topologies that differ between the BI and ML analyses. Fully supported (100/1.00) branches are marked with solid circles. Scale bar = two substitution per 100 nucleotide positions.

species, see Fig. 1. The oligotrichids *Pseudotontonia simplicidens* and *Novistrombidium orientale* and the choreotrichids *Stenosemella nivalis* and *Parastrombidinopsis minima* were selected as outgroup taxa. The alignment was initially achieved using the online program GUIDANCE 2 (Landan and Dan 2008; Medlin et al. 1988; Sela et al. 2015) with default parameters in the GUIDANCE web server (http://guidance.tau.ac.il/ver2/). The maximum likelihood (ML) analyses were conducted with RAxML-HPC2 on XSEDE (8.2.10) (Stamatakis et al. 2008) on the CIPRES Science Gateway v.3.3 (http://www.phylo.org). The program MrModeltest v.2.0 (Nylander 2004) selected GTR + I + Γ as the best model of nucleotide substitution with Akaike information criterion (AIC), which was then used for Bayesian inference (BI) analysis. The BI analysis was performed with MrBayes on XSEDE 3.2.6 (Ronquist and Huelsenbeck 2003). Markov chain Monte Carlo simulations were run with two sets of four chains for 10,000,000 generations with a sample frequency of 100 generations. The first 25% of sampled trees were discarded as burn-in prior to constructing the majority rule consensus tree. MEGA 6.0 (Kumar et al. 2018) was used to visualize the tree topologies.

ZooBank LSID

The genus *Parabistichella* Jiang et al. 2013 had previously been registered in ZooBank under urn:lsid:zoobank.org:act:352C8CD9-9DA6-4085-977D-A06A1C66090D, and its type species, *Parabistichella variabilis* Jiang et al. 2013, had previously been registered in ZooBank under urn:lsid:zoobank.org:act:F001ED12-E58B-4B37-957D-582C4A069F5F. The ZooBank registration number of the present work is: urn:lsid:zoobank.org:pub:7C73017E-FA32-4709-8E41-0152BF6F0E28.

Terminology

The general terminology and classification are according to Berger (2006, 2008) and Jiang et al. (2013). The terminology regarding the ultrastructure is mainly according to Berger (2008), Lynn (2008), Kloetzel (1974), and Foissner and Al-Rasheid (2006). Other specific terms are as follows.

Pharyngeal disks

Large accumulations of membranous bundles or small vesicles in the cytoplasm of the oral region, usually oriented perpendicularly with respect to the cortex of the oral cavity. They enable ciliates to rapidly form food tubes or food vacuole membranes, and so to exploit episodically abundant food sources (Bradbury et al. 1987; Kloetzel 1974; Lenzi and Rosati 1993).

Buccal seal

The membranous sheet observed by SEM that covers the buccal cavity. The buccal seal is very fragile and thus probably has to be restored after each feeding event (Foissner and Al-Rasheid 2006). According to Berger (2008), it is synonymous with the phago-assistant membrane observed by Sui et al. (2001) using transmission electron micrography.

Cortical granules and extrusomes

Cortical granules and *extrusomes* refer to the same structures in *P. variabilis*. The former term is used in the "Results" section, while the latter term is used in the "Discussion" after confirmation of their extrusive nature. In the figure legends, both terms are used.

RESULTS

General morphology of Shanghai population of *Parabistichella*

Cell size 150–195 × 35–50 μm in vivo, elongate-ellipsoidal in ventral and dorsal views, both ends rounded, dorsoventrally flattened with a ratio of about 2:1; body highly flexible but not contractile (Fig. 2A, B). Two subspherical to ellipsoidal macronuclear nodules in left cell half (Fig. 2F, 8A). One to eight (usually two) globular micronuclei near macronuclear nodules (Fig. 8A and Table 1). One contractile vacuole, left of midline and about 40% down length of body, about 15 μm across, pulsing at about 20 s intervals; an additional optically empty vacuole was observed in front of the contractile vacuole in a few uncompressed cells but its contraction was not observed (Fig. 2B). No obvious collecting canals recognized. In SEM, two pellicular slits (observed in four individuals), each about 3 μm long, longitudinally oriented, located between dorsal kineties 1 and 2 about 40% down length of body (Fig. 4B, D, E). Conspicuous cortical bump sometimes located on right of two slits (Fig. 4E). Series of smaller slits, each about 2 μm long and adjacent to a dorsal bristle, arranged along left side of dorsal kinety 2 (Fig. 4D). Cytopyge about 7 μm long, dorsally positioned about 85% down length of body, immediately left of dorsal kinety 2 (Fig. 4B). Excretion of waste material via cytopyge observed in some specimens (Fig. 4L). Three conspicuous cortical grooves often observed on ventral side along right marginal, midventral, and frontoventral cirral rows, respectively (Fig. 2A). Some small protrusions on right sides of marginal cirri, those along right marginal cirral row almost at right cell margin (Fig. 4F, G). Cortical granules colorless, globular, and of two types, that is, (i) the large granules (about 3 μm across) were mostly arranged along the cirral rows and dorsal kineties, and a few of them were distributed in nonciliated areas (Fig. 2D, G, H); they were argyrophilic and conspicuous in protargol preparations (Fig. 2E); (ii) the small granules (about 1 μm across) were distributed on the right side of the paroral membrane, on the left side of the endoral membrane, and in clusters to the right of several adoral membranelles (Fig. 2C, G); they were less conspicuous than the larger granules in protargol preparations (for detailed description, see "Cortical granules" in "Ultrastructure of *Parabistichella variabilis*" below). Cytoplasm colorless, usually with lipid droplets (2–4 μm across), food vacuoles (usually containing scuticociliates), and scattered crystals (Fig. 2A, B).

Adoral zone of membranelles (AZM) about one-third of body length (Fig. 2A, B, F, 4A) comprises 28–45 membranelles with cilia 12 μm long. In SEM, fourth row of each adoral membranelle usually comprises three obtuse minute cilia; cilia of first to third rows with narrowed ends (Fig. 4H). Several small intermembranellar ridges (Fig. 4I). Buccal cavity prominent; paroral inserts on buccal lip; endoral located on dorsal wall of cavity and composed of a single row of basal bodies (stichomonad) (Fig. 4A, K). Paroral and endoral almost equal in length and optically intersect in their middle regions (Fig. 2F). Three enlarged frontal cirri, with right one near distal end of AZM (Fig. 2F). Single buccal cirrus right of middle portion of paroral membrane (Fig. 2F, 4A). Midventral complex composed of 2–4 midventral pairs in typical zig-zag pattern and a midventral row consisting of 22–32 cirri that extends to rightmost transverse cirrus (Fig. 2F, 4A). One long frontoventral row with 33–49 cirri, starts near distal end of AZM and terminates near transverse cirri (Fig. 2F, 4A). Frontoterminal and pretransverse ventral cirri absent. Four to eight strong transverse cirri with cilia about 15 μm long in vivo (Fig. 2F). One left and one right marginal row composed of on average 47 and 51 cirri, respectively, with cilia about 10 μm long in vivo (Fig. 2F, 4A). Three bipolar dorsal kineties (Fig. 4B). Caudal cirri absent.

Several features, including the undulating membranes, frontoventral row, midventral complex, marginal cirral rows, and dorsal kineties, occasionally deviate from the common pattern: the paroral and endoral membranes may intersect far anteriorly rather than in their middle portions (Fig. 5B, F); the long frontoventral row may be replaced by several irregular short rows (Fig. 5A, F); one to several additional cirral rows may be present in the midventral complex (Fig. 5A, C–E, H, K, M); the marginal rows may be fragmented into several rows and one to several additional marginal cirral rows may be present

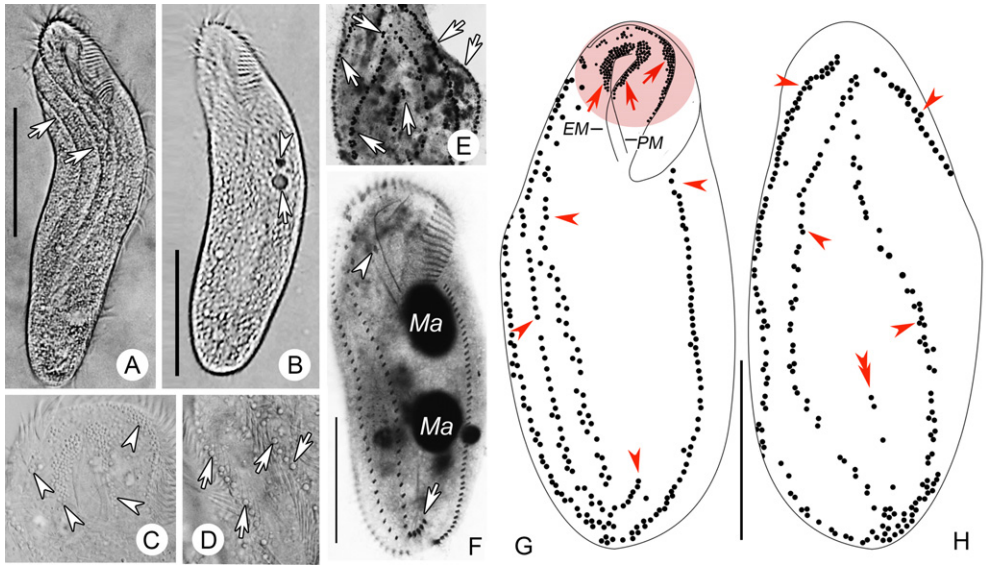

Figure 2 *Parabistichella variabilis* from life (A–D) and after protargol staining (E–H). (**A**) Ventral view of representative specimen; arrows mark cortical grooves. (**B**) Ventral view of a free-swimming individual; arrow marks the contractile vacuole, arrowhead points to extra vacuole sometimes present in front of contractile vacuole. (**C**) Anterior region showing smaller cortical granules/extrusomes (arrowheads), about 1 μm across, abundant in buccal field. (**D**) Detail of cell showing larger cortical granules (arrows), about 3 μm across, arranged along the cirral rows. (**E**) Dorsal view showing larger cortical granules (arrows) along dorsal kineties and cirral rows. (**F**) Ventral view of a representative individual, arrow shows the transverse cirri, arrowhead marks the buccal cirrus. (**G, H**) Ventral (G) and dorsal (H) views of cortical granules in a representative individual. Red circular area shows the distribution of cortical granules which were drawn from photomicrographs in vivo; arrows point to the smaller cortical granules concentrated on the right side of the paroral membrane and adoral membranelles and on the left side of the endoral membrane; arrowheads mark the larger cortical granules arranged along cirral rows and dorsal kineties; double-arrowheads show several larger cortical granules in the glabrous area between dorsal kineties 2 and 3 in posterior half of cell. EM = endoral membrane; Ma = Macronuclear nodule; PM = paroral membrane. Scale bars = 50 μm.

(Fig. 5A, C, D, J, L); a short additional dorsal kinety row may also be present (Fig. 5I). These variations are not included in Table 1.

Ultrastructure of *Parabistichella variabilis*

Pellicle of somatic region

The pellicle comprises the plasma membrane and alveoli subtended by a single longitudinal microtubular layer (Fig. 6A, B). No clear perilemma or epiplasm were observed in cell sections.

Cortical granules

In SEM, numerous ellipsoidal or ovoidal extruded granules (about 1.5 μm × 0.6 μm) were observed to extend beyond the cell surface to the left of the marginal and midventral cirri (Fig. 7B), near the transverse cirri (Fig. 7C), around the dorsal cilia (Fig. 7A, D, H, I), and in the glabrous stripe between dorsal kineties 2 and 3 in the posterior half of cell (Fig. 2G, H, 7A), that is, with a similar arrangement to the large cortical granules observed by light microscopy. The surface of extruded granules was uneven, and sometimes the residual "pits" were visible (Fig. 7D, H, I, F). Several granules about 1 μm across were scattered in the cortex of the buccal field and occasionally near the bases of the adoral membranelles and the undulating membranes, that is, with a similar arrangement to the small cortical granules observed by light microscopy (Fig. 7E, G). In TEM, the cortical granules were mostly located in the cortex and each was bounded by a single membrane; they were either grouped around the cirri (Fig. 6C, F), arranged in longitudinal rows (Fig. 6D), concentrated near the intermembranellar ridges (Fig. 3A), or densely distributed in the buccal field (Fig. 3D, J). The largest cortical granules observed by TEM were about 1.5 μm across in the somatic region, but only about 0.5 μm across in the buccal field (Fig. 3D, 6E), which was consistent with the results of light microscopy and SEM. The cortical granules had a highly electron-dense core, circular in cross-section, surrounded by an electron-lucent layer about 0.1 μm thick (Fig. 6E). In cortical granules that were fused with the pellicle, the margin of the highly electron-dense material was not well defined (Fig. 6G–I).

Structures in buccal field

The paroral membrane and the remains of the buccal seal (which was about 0.3–1 μm in thickness) were observed by SEM (Fig. 4J, K). In TEM, the buccal seal and the left wall of the buccal lip were both bounded by the plasma membrane and contain numerous small cytoplasmic vesicles; a single layer of longitudinal microtubules is present in the buccal seal only (Fig. 3E–I). The nematodesmata originating from the adoral membranelles

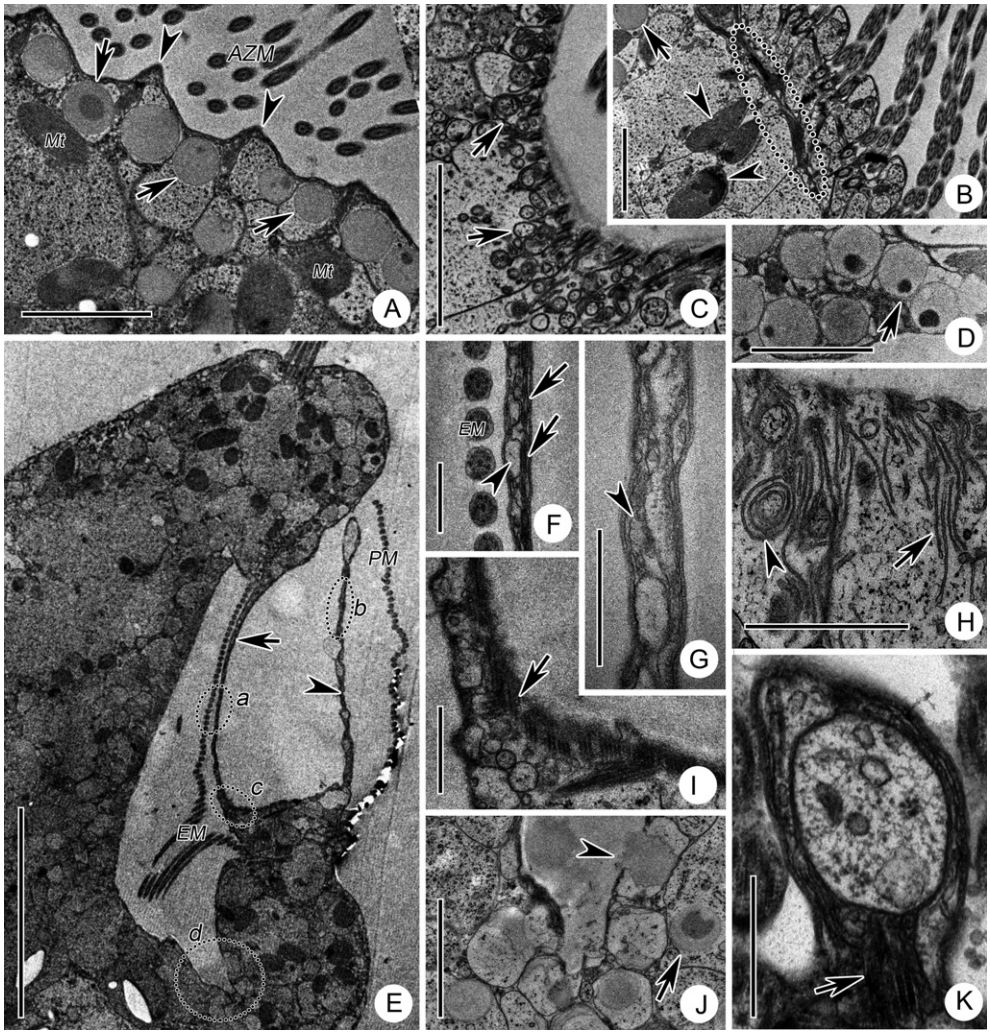

Figure 3 Transmission electron micrographs showing structures in buccal field of *Parabistichella variabilis*. (**A**) Cortical granules (extrusomes) (arrows) concentrated near intermembranellar ridges (arrowheads). (**B**) Cross-sections of oral area containing adoral zone of membranelles (AZM), showing fiber bundles of membranellar cilia (circle), extrusomes (arrows) and mitochondria (arrowheads). (**C**) Section perpendicular to pellicle showing thread-shaped pharyngeal disks (arrows) in buccal field. (**D**) Extrusomes (arrows) compacted below the pellicle. (**E**) Longitudinal section of buccal field, showing the left wall of the buccal lip (arrowhead) near the paroral membrane (PM) and the buccal seal (arrow) near the endoral membrane (EM); areas marked "a" "b" "c" and "d" are enlarged in F, G, I and J, respectively. (**F**) The buccal seal is bounded by the plasma membrane and contains numerous small cytoplasmic vesicles (arrowhead), arrows mark the single layer of longitudinal microtubules. (**G**) The left wall of buccal lip contains numerous small cytoplasmic vesicles (arrowhead) and is bounded by the plasma membrane. (**H**) Pharyngeal disks with different shapes, that is, thread-shaped (arrow) and ring-shaped (arrowhead), located in cortex of buccal cavity. (**I**) Base of buccal seal, showing the microtubules (arrow) located beneath pellicle and longitudinally extended to the rest of buccal seal. (**J**) Deep area of buccal cavity, arrow marks extrusome below pellicle, arrowhead points to an extruding extrusome. (**K**) Conspicuous fibers (arrow) in the evaginated pellicular ridges between two adjacent adoral membranelles. AZM = adoral zone of membranelles; EM = endoral membrane; Mt = mitochondria; PM = paroral membrane. Scale bars = 1 μm (A, D, H, I), 5 μm (B), 2 μm (C), 10 μm (E) and 0.5 μm (F, G, I–K).

form the submembranellar fibers (Fig. 3B). Intermembranellar fibers were present in the intermembranellar ridges (Fig. 3K). A large number of densely arranged pharyngeal disks were present in the cortex, either beneath the dorsal wall of the buccal cavity near the pellicle or in the cytoplasm distant from the pellicle (Fig. 3C, H). Those near the pellicle appeared as flattened vesicles comprising an electron-dense contents surrounded by a single membrane and were oriented orthogonal to the cell surface (Fig. 3C, H); those scattered in the cytoplasm were curved and appeared either as single or concentric rings (Fig. 3H).

Cytoplasm, other cytoplasmic organelles, and nuclear apparatus

The cytoplasm of *P. variabilis* had an electron-lucent colloidal appearance and contained numerous irregularly shaped vesicles of various sizes and with low electron

Table 1. Morphometric characterization of *Parabistichella variabilis* Shanghai population

Character	Min	Max	Mean	M	SD	CV	*n*
Length of body	118	184	152.9	150	20.70	13.5	20
Width of body	35	76	60.5	60	10.97	18.1	20
Ratio of body length: body width	2.0	3.5	2.6	2.5	0.33	12.9	20
Length of adoral zone	42	73	51.6	51	8.10	15.7	20
Ratio of AZM length: body length	0.3	0.4	0.3	0.3	0.03	8.3	20
Anterior body end to paroral membrane: distance	5	15	10.4	11	2.54	24.5	20
Anterior body end to endoral membrane: distance	8	15	10.3	10	1.98	19.2	20
Anterior body end to buccal cirrus: distance	20	35	27.4	28	4.31	15.7	20
Number of adoral membranelles	28	45	34.0	34	3.95	11.6	20
Number of buccal cirri	1	1	1.0	1	0	0	20
Number of frontal cirri	3	3	3.0	3	0	0	20
Number of transverse cirri	4	8	6.3	6	1.03	16.4	20
Number of midventral pairs	2	4	2.4	2	0.59	25.0	20
Number of cirri in midventral row	22	32	27.6	28	2.86	10.4	20
Number of cirri in frontoventral row	33	49	39.1	39	4.77	12.2	20
Number of right marginal rows	1	2	1.1	1	–	–	20
Number of cirri in right marginal row	32	77	51.5	50	10.94	21.2	19
Number of left marginal rows	1	2	1.1	1	–	–	20
Number of cirri in left marginal row	41	62	47.3	46	5.18	11.0	19
Number of dorsal kineties	3	4	3.1	3	–	–	18
Number of macronuclear nodules	2	2	2.0	2	0	0	20
Length of anterior macronuclear nodule	17	33	27.3	29	4.23	15.5	20
Width of anterior macronuclear nodule	12	19	14.6	15	1.64	11.2	20
Number of micronuclei	1	8	2.8	2	2.25	81.9	8
Length of micronuclei	3	5	3.8	4	0.89	23.6	8
Width of micronuclei	2	4	3.1	3	0.64	20.5	8

All data are based on protargol-stained specimens, measurements in μm.
AZM = adoral zone of membranelles; CV = coefficient of variation in %; M = median; Max = maximum; Mean = arithmetic mean; Min = minimum; *n* = sample size; SD = standard deviation.

density. Mitochondria, cortical granules, and the cytoplasmic matrix were all surrounded by these vesicles (Fig. 8A). Each macronuclear nodule was surrounded by a karyotheca and contains various chromatin bodies and several spherical nucleoli (Fig. 8A, C). The chromatin bodies were 0.1–0.8 μm in diameter and are of homogeneous high electron density, whereas the nucleoli were larger (about 1–2 μm in diameter) and contained several electron-dense particles (Fig. 8A, C). The micronuclei contained numerous chromatin bodies of homogenous electron density (Fig. 8A, B).

Ontogenesis of Shanghai population of *Parabistichella variabilis*

The description here is restricted to early-to-middle stages as the late stages have been reported previously (Jiang et al. 2013). (1) In the opisthe, the oral primordium originates de novo (Fig. 9A). (2) In the proter, the posterior portions of both the parental adoral zone and the parental undulating membranes are reorganized (Fig. 9B–D). (3) Some posterior cirri of the midventral row dedifferentiate and join the oral primordium, and the transverse cirri partly dedifferentiate (Fig. 9B–D). (4) The parental midventral and frontoventral rows participate in the formation of the frontoventral-transverse cirral anlagen of both the proter and opisthe (Fig. 9B, C). (5) The marginal cirral anlagen develop intrakinetally (Fig. 9D). (6) The anlagen of the dorsal kineties develop intrakinetally.

SSU rDNA sequence and phylogenetic analyses

The SSU rDNA sequence of the Shanghai population of *Parabistichella variabilis* is deposited in the GenBank database with the accession number, length, and GC content as follows: MK809247, 1,729 bp, 45.63%.

The SSU rDNA sequence similarity between *P. variabilis* and related taxa was analyzed. The SSU rDNA sequences of the two Chinese populations of *P. variabilis* (Guangzhou and Shanghai) are identical. The sequence similarities of *P. variabilis* (Guangzhou and Shanghai populations) to *Uroleptoides magnigranulosus*, *Orthoamphisiella* sp., *O. breviseries*, *Lamtostyla salina*, *L. ovalis*, *Bistichella cystiformans* or *B. variabilis* were in the range of 99.30–99.88%.

The ML and BI trees had similar topologies, therefore, only the ML tree is shown here with support values at the nodes from both algorithms (Fig. 1). The two populations of *P. variabilis* (Guangzhou and Shanghai) cluster together with moderate to high support (ML/BI, 90/1.00), forming a clade that is sister to *Uroleptoides magnigranulosus*. This

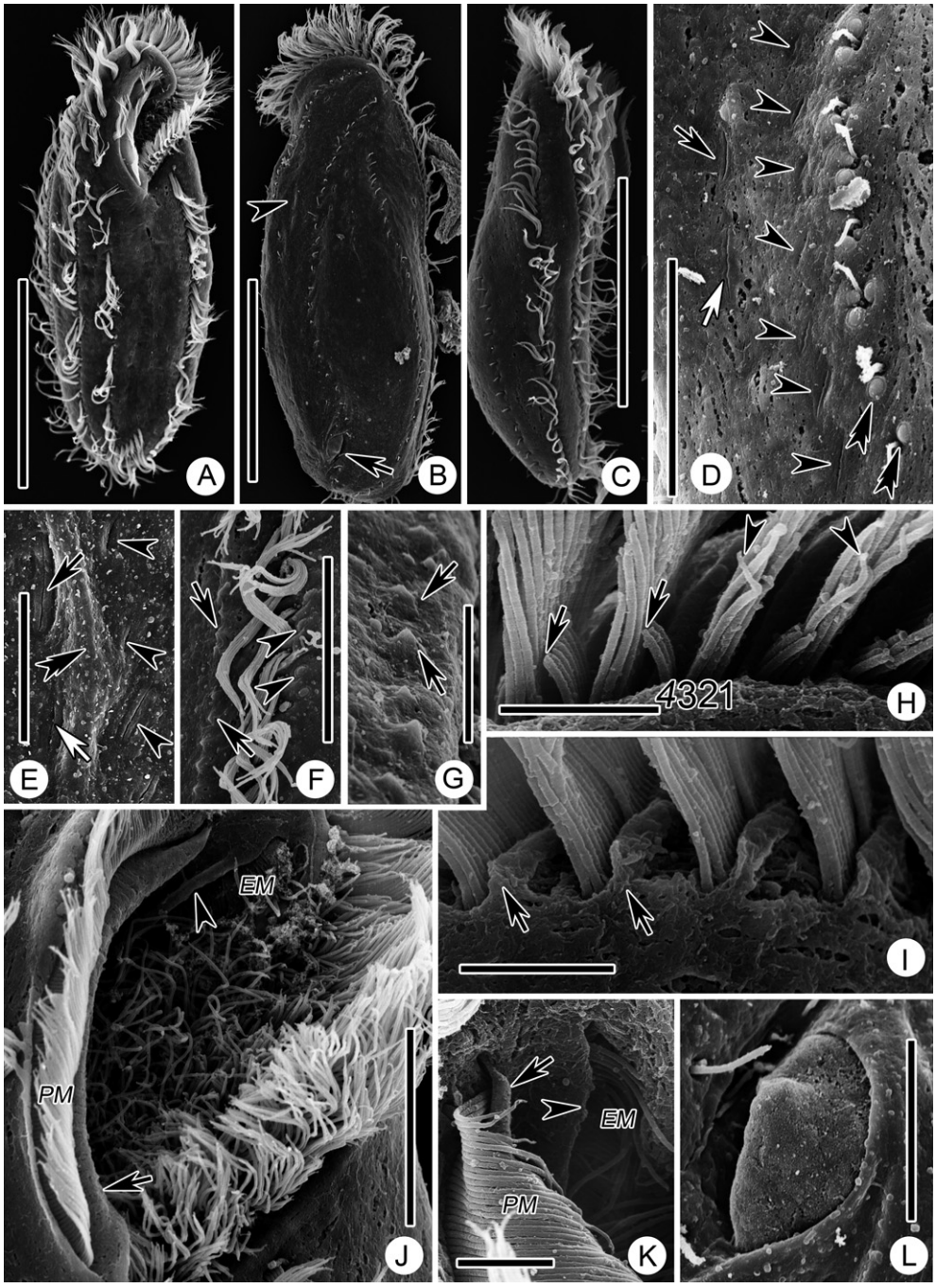

Figure 4 Scanning electron micrographs of *Parabistichella variabilis*. (**A, B**) Ventral view (A) and dorsal view (B) of representative individuals, arrow shows cytopyge and arrowhead marks contractile vacuole pore. (**C**) Right lateral view of representative individual. (**D**) Two pellicular slits which are possibly contractile vacuole pores (arrows), and series of smaller-sized slits (arrowheads) located between dorsal kineties 1 and 2; double-arrowheads mark the extrusomes. (**E**) Pellicular bump (double-arrowheads) which is sometimes present between larger slits (arrows) and smaller slits (arrowheads). (**F, G**) Small ridges (arrows) located along left side of left (F) and right (G) marginal cirral rows; arrowheads show extrusomes. (**H**) Anterior portion of adoral zone, to show differentiation of membranellar cilia of AZM: minute cilia (arrows) in row 4; cilia with narrowed ends (arrowheads) situated in rows 1–3 forming a membranelle; numbers mark scheme of cilia in adoral membranelles composed of four rows. (**I**) Dorsal view of intermembranellar ridges (arrows) between adoral membranelles. (**J, K**) Buccal region, arrow marks the right wall of buccal lip, arrowhead points to residuum of buccal seal. (**L**) Cytopyge during expulsion of waste material. EM = endoral membrane; PM = paroral membrane. Scale bars = 50 μm (A–C), 10 μm (D, J), 5 μm (E–G) and 2.5 μm (H, I, K, L).

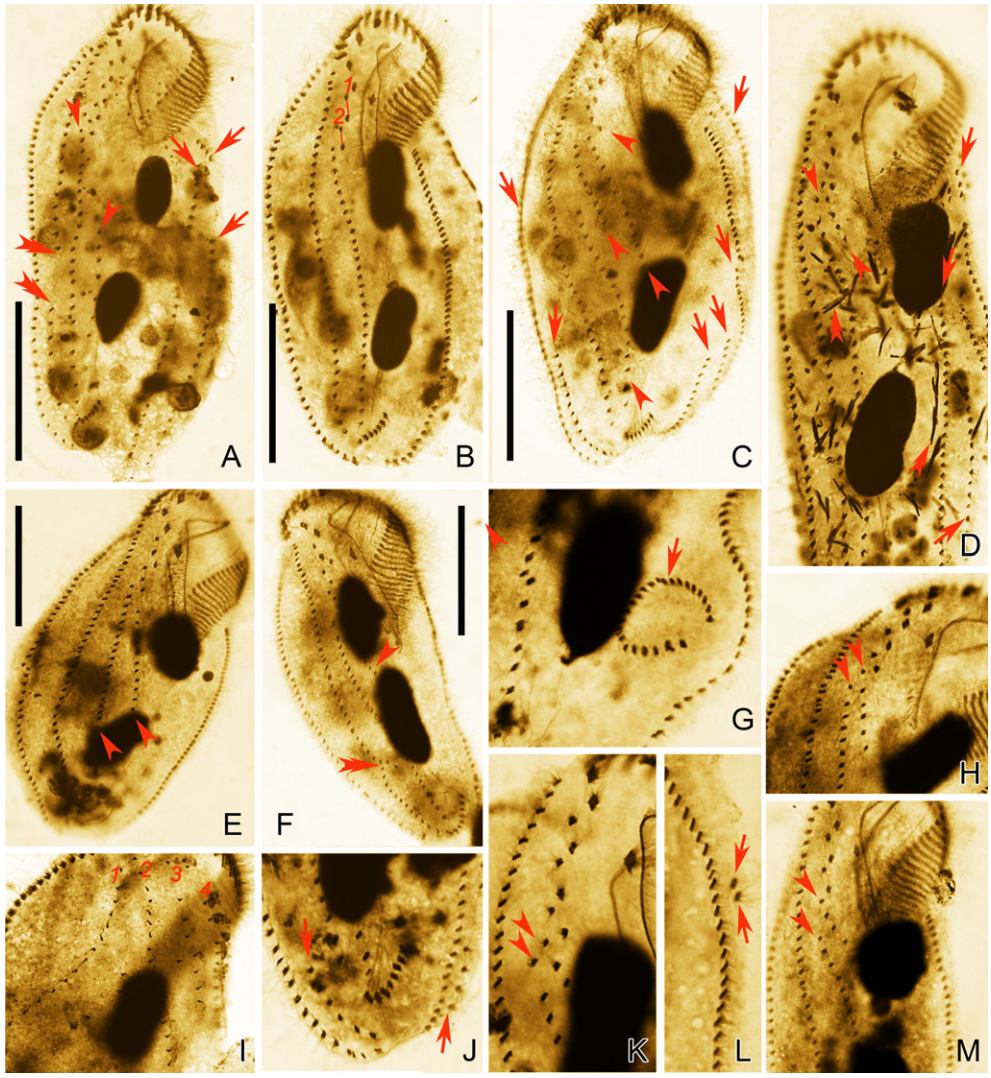

Figure 5 Photomicrographs of *Parabistichella variabilis* after protargol staining to show variation in the infraciliature. (**A**) Individual with additional left marginal rows (arrows), additional midventral rows (arrowheads), and fragmented frontoventral rows (double-arrowheads). (**B**) Individual with two midventral pairs (1, 2), paroral and endoral membranes intersect in their anterior rather than their middle portion. (**C**) Individual with additional fragmented marginal rows (arrows) and midventral rows (arrowheads). (**D**) Individual with additional midventral rows (arrowheads) and marginal rows (arrows), double-arrowheads point to ingested algae. (**E, H, K, M**) Individuals with additional midventral rows (arrowheads). (**F**) Individual with multiple morphological variations, that is, fragmented frontoventral rows (double-arrowheads), additional midventral rows (arrowheads); paroral and endoral membranes intersect in anterior rather than middle region. (**G, J**) Individuals with additional marginal rows (arrows). (**I**) Individuals with additional dorsal kinety. (**L**) Individuals with additional marginal cirri (arrows). Scale bars = 50 μm.

indicates a close relationship of these two species, which is consistent with previous findings (Jiang et al. 2013).

DISCUSSION

General morphological and ontogenetic comparison of Shanghai and Guangzhou populations of *Parabistichella variabilis*

The genus *Parabistichella* was established by Jiang et al. (2013) with *P. variabilis* as the type species. The Shanghai population matches the Guangzhou population well in terms of the nuclear apparatus and cirral pattern (Jiang et al. 2013). However, the former differs from the latter in having: (i) a more slender body in vivo (35–50 μm vs. 65–85 μm in width); (ii) fewer adoral membranelles (34 vs. 47 on average) and frontoventral cirri (39 vs. 61 on average); (iii) more right marginal cirri (52 vs. 47 on average); and (iv) smaller cortical granules in the buccal field (1 μm vs. 3 μm across). Furthermore, the Shanghai population displays a variability not observed in the Guangzhou population concerning: (i) the position of the optical intersection of paroral and endoral; (ii) the presence of a short additional dorsal kinety row; and (iii) the fragmentation of the

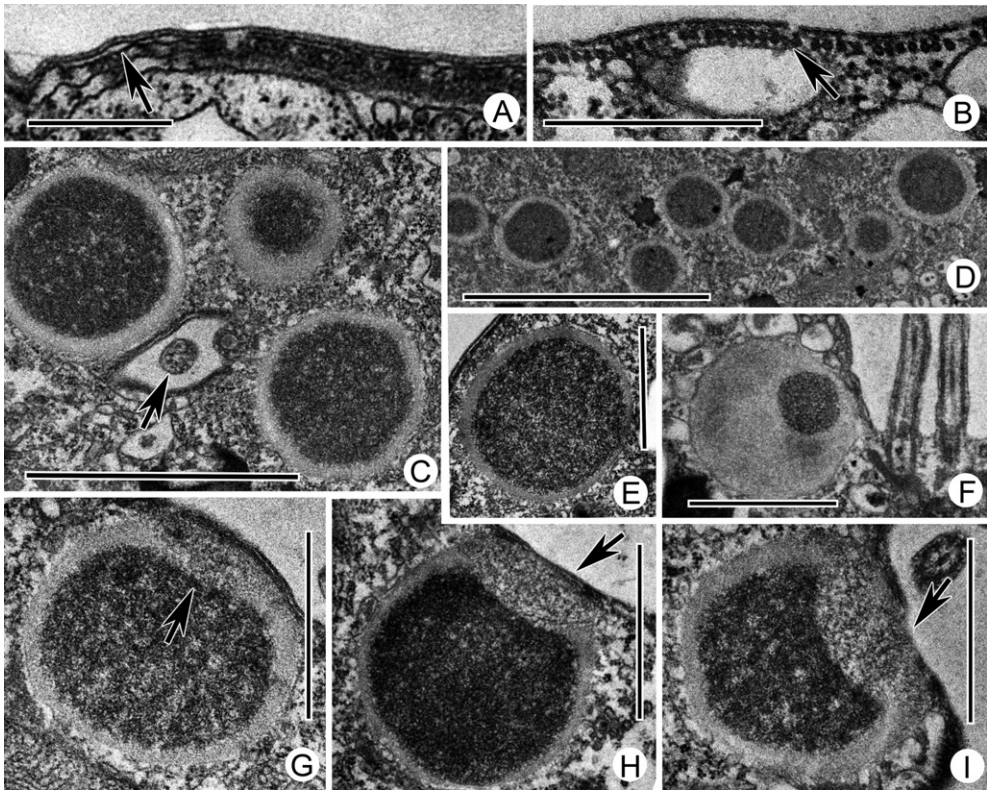

Figure 6 Transmission electron micrographs of cortex of *Parabistichella variabilis*. (**A**) Pellicle composed of plasmalemma and alveoli (arrow). (**B**) Cortex region, showing subpellicular microtubule layer (arrow). (**C**) Section parallel to pellicle showing cortical granules (extrusomes) grouped around dorsal bristle (arrow). (**D**) Section parallel to pellicle showing arrangement of extrusomes in glabrous area. (**E**) Single extrusome, to show electron-dense core and electron-lucent surrounding layer. (**F**) Extrusome located near cirri. (**G–I**) Section perpendicular to pellicle showing extrusomes possibly in early stages of extrusion and structural change in the part close to pellicle; arrows in G and H mark area of depolymerization and in I points to fusion of extrusome membrane with pellicle. Scale bars = 5 μm (A, D), 10 μm (B), 2 μm (C) and 1 μm (E–I).

marginal rows. Since the two populations overlap in their morphometric ranges concerning the numbers of adoral membranelles, frontoventral cirri, and right marginal cirri, we consider these differences to be intraspecific variability caused by environmental conditions, hence, the conspecificity of the two populations is beyond reasonable doubt.

The middle-to-late stages of ontogenesis in the Shanghai population of *P. variabilis* are consistent with those reported by Jiang et al. (2013) for the Guangzhou population (data not shown). The present study provides the first description of early-to-middle stages and thus completes the characterization of the ontogenic process for this species.

New structures observed by SEM in *Parabistichella variabilis*

The contractile vacuole can usually easily be observed in live hypotrich ciliates (Berger 1999, 2006, 2008). However, the position and shape of the contractile vacuole pore have rarely been reported, even by SEM (Foissner and Stoeck 2011). In our study, two longitudinal pellicular slits were observed between the dorsal kineties 1 and 2. They are close to the contractile vacuole and are morphologically similar to the slit-like contractile vacuole pores in *Cotterillia bromelicola*, *Metopus murrayensis*, *Urosoma emarginata*, and *Urosoma salmastra* (Dong et al. 2020; Foissner and Stoeck 2011; Vd'ačný and Foissner 2017). Therefore, these two slits might represent the contractile vacuole pores of *Parabistichella variabilis*. Most hypotrichs have a single contractile vacuole although some (e.g. *Sterkiella admirabilis*, *Onychodromus quadricornutus*, *Hemicycliostyla sphagni*, *Hemisincirra vermicularis*, and *Circinella vettersi*) may have two to several (Berger 1999, 2006, 2008, 2011). It is noteworthy that the existence of two contractile vacuole pores, together with an additional vacuole sometimes observed in front of the contractile vacuole in vivo, suggest that *P. variabilis* might actually have two contractile vacuoles rather than one as reported in Jiang et al. (2013). The contractile vacuole pores in non-hypotrich ciliates (e.g. Peniculida and Gymnostomatida) are usually circular (Foissner 2016; Foissner et al. 2002; Xu et al. 2018), whereas the data available suggest that contractile vacuole pores in hypotrichs might be typically slit-like (Dong et al. 2020; Foissner and Stoeck 2011). The series of smaller pellicular slits along the left side of dorsal kinety 2 have not been reported previously. Further studies by SEM and TEM are needed in order to determine the structure and function of these slits.

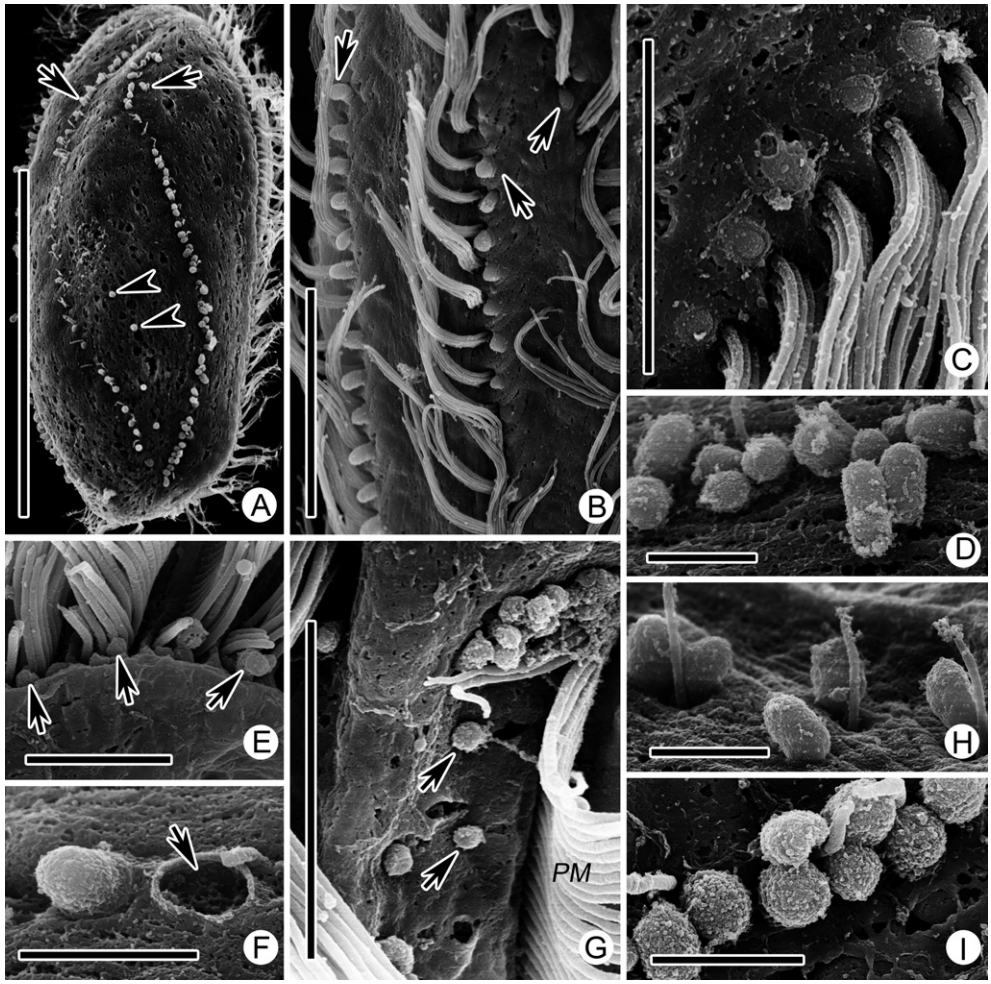

Figure 7 Scanning electron micrographs showing extruded cortical granules (extrusomes) of *Parabistichella variabilis*. (**A**) Dorsal view of cell, to show extruded structures in clusters with dorsal bristles (arrows), arrowheads mark the larger extrusomes loosely arranged in a longitudinal line in the posterior half of the cell in the glabrous area between dorsal kineties 2 and 3. (**B, C**) Ventral views, to show arrangement of extruding extrusomes (arrows in B) on right base of right marginal cirri (B), midventral complex (B) and near the transverse cirri (C). (**D, H**) Extruded extrusomes in lateral views, grouped around dorsal cilia. (**E, G**) Smaller-size extruded extrusomes (arrows) in buccal area (near adoral zone of membranelles in E, and near paroral membrane in G). (**F**) Residual "pit" (arrow) after extrusome has been extruded. (**I**) Apical view of extruded extrusomes. PM = paroral membrane. Scale bars = 50 μm (A), 10 μm (B), 5 μm (C, E, G) and 2 μm (D, F, H, I).

The buccal seal was generally overlooked in hypotrichs until Foissner and Al-Rasheid (2006) demonstrated its presence in more than 40 hypotrich species based on SEM studies. Three types of buccal seal were described by Foissner and Al-Rasheid (2006): (i) the most common type, in which the seal covers the oral opening, the lateral membranellar cilia, and the proximal portions of the adoral membranelles; (ii) the deeper type, found only in *Pleurotricha lanceolata,* which covers neither the lateral membranellar cilia nor the bases of the adoral membranelles; and (iii) the complex type, which is found in species with a deep buccal cavity, for example, *Cyrtohymena candens* and *Saudithrix terricola*, and comprises an upper and a lower seal. Our results suggest that the buccal seal of *Parabistichella variabilis* probably belongs to one of the first two types because only a small remnant of membrane-bound structure was observed attached to the inner part of the buccal lip, making it difficult to determine whether it covers the lateral membranellar cilia and the proximal portion of the adoral membranelles. Sui et al. (2001) described two phago-assistant membranes made of microtubules located between the paroral and endoral membranes in *Stylonychia mytilus*, which were considered to be synonymous with the buccal seal (Berger 2008). Our observations of *P. variabilis* also show microtubules within the buccal seal. We agree with Berger's opinion since the buccal seal and the phago-assistant membrane have same location and similar structure. We speculate that the buccal seal of hypotrichs is an extension of the pellicle of the buccal cavity wall, although Foissner and Al-Rasheid (2006) considered the buccal seal to be a very fragile structure that is easily destroyed. In

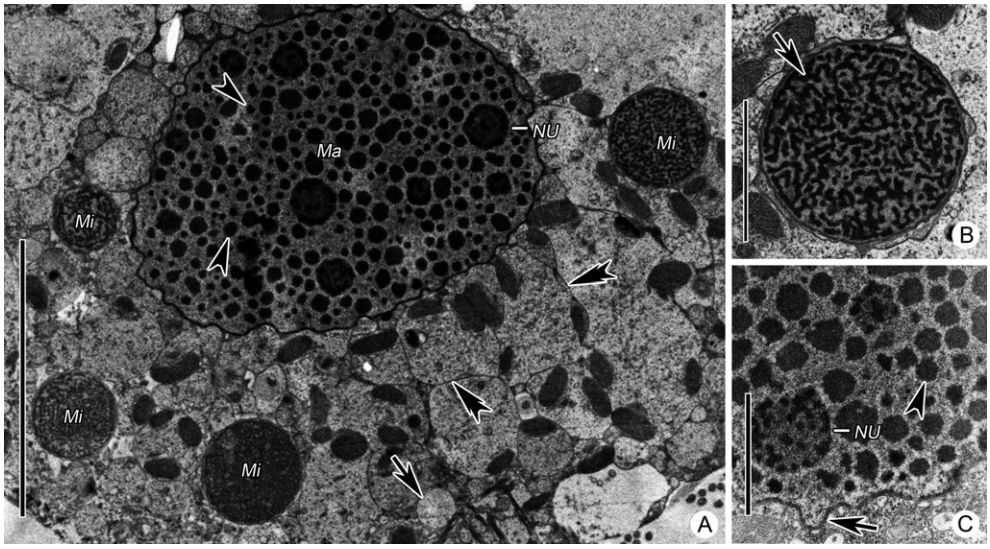

Figure 8 Transmission electron micrographs showing structures in cytoplasm of *Parabistichella variabilis*. (**A**) Micronucleus, macronuclear nodule containing chromatin bodies (arrowheads) and nucleoli, vesicles containing cytoplasm matrix (double-arrowheads) and extrusomes (arrow). (**B**) Micronucleus, arrow shows the electron-dense chromatin. (**C**) Part of macronuclear nodule, to show the karyotheca (arrow), chromatin bodies (arrowheads), and nucleoli. Ma = Macronuclear nodule; Mi = micronucleus; NU = nucleolus. Scale bars = 10 μm (A) and 2 μm (B, C).

their TEM investigation of *Stylonychia mytilus*, Sui et al. (2001) reported that one of the "phago-assistant membranes" is located near the endoral and the other is located on the left side of the buccal cavity. After carefully comparing these structures with the buccal seal of *S. mytilus* observed by Foissner and Al-Rasheid (2006) using SEM, we conclude that, other than the left wall of the buccal lip, the only the structure near the endoral was the buccal seal.

Ultrastructural features of pellicle

The pellicle in ciliates is typically composed of the plasma membrane, alveoli, and often the closely apposed underlying fibrous epiplasm (Lynn 2008). The perilemma is an additional "unit membrane-like" structure covering the pellicle (Lynn 2008). Although it has been reported in some species of hypotrich ciliates (Bardele 1981; Carey and Tatchell 1983; Dong et al. 2020; Foissner et al. 2007; Wirnsberger-Aescht et al. 1989), the perilemma might be absent in others (Grim 1972; Jerka-Dziadosz 1982; Wirnsberger and Hausmann 1988). No perilemma was observed in any region of the cell of *P. variabilis*. Fixation is a well-known problem in TEM preparations of hypotrichs (Shigenaka et al. 1973). It is therefore unclear whether its absence in *P. variabilis* is a fixation artifact.

Longitudinally oriented subpellicular microtubules that extend just beneath the pellicle have frequently been reported in hypotrichs (Fleury 1988; Grimes 1972; Wirnsberger-Aescht et al. 1989). Berger (1999) discussed the correlation between body rigidity and the arrangement of the subpellicular microtubules, that is, species with a rigid body, such as *Stylongchia mytilus* and *Histriculus similis*, have subpellicular microtubules arranged in crosswise layers, whereas species with a flexible body, such as *Oxytricha fallax* and *Engelmanniella mobilis*, have only a single layer of subpellicular microtubules (Calvo et al. 1986; de Puytorac et al. 1976; Grimes 1972; Wirnsberger-Aescht et al. 1989). In *P. variabilis*, which has a flexible body, the subpellicular microtubules are arranged in a single layer parallel to the surface of the cell, which supports the hypothesis of Berger (1999).

Cortical granules of *Parabistichella variabilis* are mucocysts

The cortical granules of *P. variabilis* are extrusomes (extrusive organelles) according to the definition given by Hausmann (1978), that is, they are membrane-bound organelles that can be extruded and expel their contents to the outside of the cell.

In the Hypotrichia, five types of extrusomes have been reported, although information on their ultrastructure is limited and can be summarized as follows: (1) trichocyst-like extrusomes with four different electron-dense parts (cap, tip, body, and central shaft), for example, in *Pseudourostyla nova*, *P. cristata*, and *Anteholosticha monilata* (Zhang et al. 2011, 2012; Zhou et al. 2011); (2) pigmentocysts, which are globular and always contain a very electron-dense "core", for example, in *Pseudokeronopsis carnea* (Wirnsberger and Hausmann 1988); (3) typical mucocysts, which are composed of two parts (tip and body) with different electron-dense crystal material, for example, in *Urostyla grandis* (Zhang et al. 2007); (4) prolate elliptical extrusomes, which probably represent a kind of mucocyst, for example, in *Urosoma emarginata* (Dong et al. 2020); and (5) cup-shaped mucocysts, which comprise a globular electron-lucent cavity while the rest of the

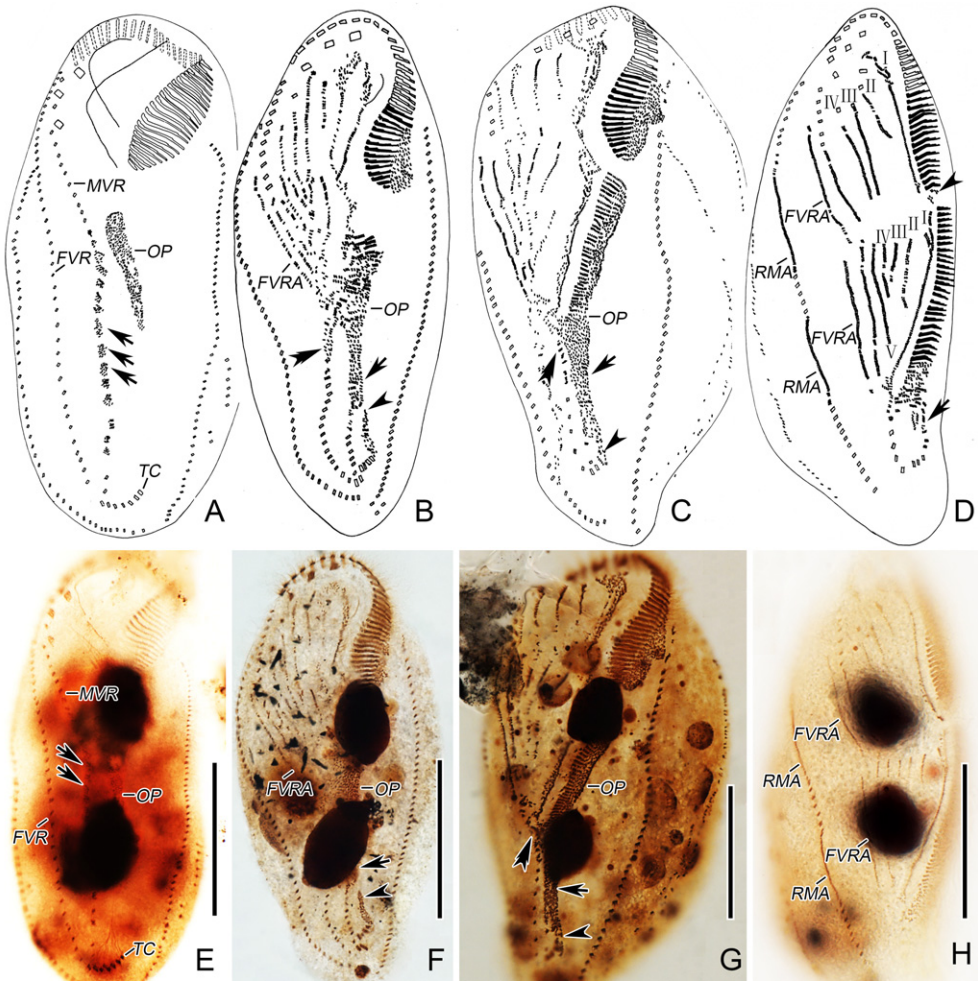

Figure 9 Early-to-mid stages of ontogenesis in *Parabistichella variabilis* after protargol staining. (**A, E**) Ventral views of an early divider, to show oral primordium and dedifferentiation of old midventral row (arrows). (**B, F**) Ventral views of early divider, to show dedifferentiation of old frontoventral row (double-arrowheads), midventral row (arrows), and transverse cirri (arrowheads). (**C, G**) Slightly later stage showing frontoventral-transverse cirral anlagen, the new oral apparatus of the opisthe starting to organize, and dedifferentiation of the old frontoventral row (double-arrowheads), midventral row (arrows), and transverse cirri (arrowhead). (**D, H**) Divider in following stage, to show streaks of frontoventral-transverse cirral anlagen (I–V), the right marginal row anlage and frontoventral row anlage; arrowhead indicates the reorganization of old adoral membranelles; arrow denotes dedifferentiating old transverse cirri. FVR = frontoventral row; FVRA = frontoventral row anlage; I–V = frontoventral-transverse cirral anlagen; MVR = midventral row; OP = oral primordium; RMA = right marginal row anlage; TC = transverse cirri. Scale bars = 50 μm.

structure is composed of very electron-dense material, for example, in *Oxytricha granulifera* and *Architricha indica* (Tang et al. 2016; Zhang et al. 2014). The globular extrusomes of *P. variabilis* have a heterogeneous content similar to that of the "typical" (type 3) and cup-shaped mucocysts (type 5). However, the extrusomes in *P. variabilis* differ from both in terms of their size and shape. Furthermore, the structure of the extrusomes in *P. variabilis*, which comprises a very electron-dense core surrounded by a thin layer of electron-lucent material, resembles that of the extrusomes in *U. emarginata*, although their shapes (globular vs. elliptical) and surfaces (decorated by spiraling ribs vs. irregular) differ significantly. Thus, the extrusomes of *P. variabilis* probably represent a new kind of mucocyst. Extrusomes fusing with the pellicle are characterized by a deviating inner structure (Fig. 6G–I), therefore, the presence of such a structure might indicate that the mucocyst is mature and ready for extrusion. Further TEM-based investigations on this type of mucocyst are needed in order to fully characterize it and determine its function.

Ultrastructural features of pharyngeal disks

The pharyngeal disks, also called membrane-packed disks, are precursors in the wall of the buccal cavity that rapidly form food vacuole membranes. They have been reported in several groups of filter-feeding ciliates (e.g. *Ascophrys* sp., *Euplotes* sp., *Certesia quadrinucleata*) (Bradbury et al.

1987; Kloetzel 1974; Verni and Gualtieri 1997; Wicklow 1983). Here, we classify the different types of pharyngeal disks reported in the literature according to their structure and electron density as follows: (1) single-membrane-bound pharyngeal disks that are comparatively electron-lucent, for example, in *Euplotidium itoi*, *Climacostomum virens*, and *Uronychia transfuga* (Fischer-Defoy and Hausmann 1981; Lenzi and Rosati 1993; Morelli et al. 1996) and (2) myeloid pharyngeal disks, which are very electron-dense, have multiple lamellar membranes, and may be rod- or ring-shaped, for example, in *Euplotes eurystomus*, *Certesia quadrinucleata*, *Diophrys oligothrix*, and *D. scutum* (Fauré-Fremiet and André 1968; Gong et al. 2018; Kloetzel 1974; Rosati et al. 1987; Verni and Gualtieri 1997; Wicklow 1983). The single-membrane-bound type is present in *P. variabilis*.

Taxonomy and systematics of *Parabistichella*

When it was first described, the genus *Parabistichella* Jiang et al. 2013, was considered incertae sedis in the hypotrichs (Jiang et al. 2013). Here, we sequenced another population of *Parabistichella* and, using a broad selection of SSU rDNA sequences that we analysed by both ML and BI, constructed phylogenetic trees to investigate the systematic position of *Parabistichella*. In both analyses, the Shanghai population of *P. variabilis* is closely related to the Guangzhou population which together have a close relationship with species from different genera such as *Orthoamphisiella breviseries*, *Uroleptoides magnigranulosus*, and *Tachysoma pellionellum*. These findings are consistent with previous studies, although *Parabistichella* was not the focus of those studies (Dong et al. 2016; Fan et al. 2014; Jiang et al. 2013; Luo et al. 2019; Moon et al. 2019; Park et al. 2017).

Foissner (2016) expanded the genus *Parabistichella* by describing one novel species (*Parabistichella bergeri*) and transferring five species from other genera. The genus now comprises the following species: *P. variabilis* Jiang et al. 2013 (type species); *P. bergeri* Foissner 2016, *P. cystiformans* (Fan et al. 2014) Foissner 2016 (original combination: *Bistichella cystiformans* Fan et al. 2014); *P. dieckmanni* (Foissner 1998) Foissner 2016 (original combination: *Keronopsis dieckmanni* Foissner 1998); *P. namibiensis* (Foissner et al. 2002) Foissner 2016 (original combination: *Amphisiella namibiensis* Foissner et al. 2002; synonym *Bistichella namibiensis* (Foissner et al. 2002) Berger 2008); *P. procerus* (Berger and Foissner 1987) Foissner 2016 (original combination: *Pseudouroleptus procerus* Berger and Foissner 1987; synonym *Bistichella procerus* (Berger and Foissner 1987) Berger 2008); *P. terrestris* (Hemberger 1985) Foissner 2016 (original combination: *Pseudouroleptus terrestris* Hemberger 1985; synonym *Bistichella terrestris* (Hemberger 1985) Berger 2008).

It is widely accepted that extrusomes are reliable characters for determining taxonomic and phylogenetic affinities in many ciliate groups (Bannister 1972; Dallai and Luporini 1981; Eisler and Peck 1998; Görtz 1982; Rosati and Modeo 2003; Roth 1957; Wessenberg and Antipa 1970). However, the present study reveals that only the type species, *P. variabilis*, possesses distinct cortical granules, shown here to be extrusomes, whereas all congeners lack cortical granules/extrusomes. Furthermore, *P. cystiformans* (KJ509196) did not cluster with *P. variabilis* (JN008943 and MK809247) in the SSU rDNA tree but occupied the basal position in the clade that comprised species of *Uroleptoides*, *Orthoamphisiella*, *Lamtostyla*, *Bistichella*, and *Tachysoma* (Fig. 1). Thus, the present generic affiliations of *P. cystiformans* and the five species transferred to *Parabistichella* by Foissner (2016) are doubtful, pending the availability of ultrastructural and gene sequence data for other species of this genus.

A major constraint of the present analyses is the limited availability of molecular data for certain taxa, specifically *Orthoamphisiella,* for which only three sequences are available, that is, two for *O. breviseries* and one for an unidentified species but none for the type species *O. stramenticola*. Consequently, the systematic position of the genus *Orthoamphisiella* remains uncertain (Berger 2011; Huang et al. 2016). Moreover, members of this genus differ distinctly from those of *Parabistichella* in having no, or only one, long frontoventral row (vs. two or three), and the frontoventral row of the proter being composed of a combination of parental and newly formed cirri (vs. newly formed cirri only). Therefore, it is unlikely that *Parabistichella* and *Orthoamphisiella* belong to the same family (Eigner and Foissner 1991; Fan et al. 2014). The genus *Tachysoma,* for which only one sequence is available, that is, *T. pellionellum* KM222096, has the typical 18 frontal-ventral-transverse cirral pattern, dorsomarginal kineties, a flexible body, and dorsal kineties fragmentation during morphogenesis, suggesting a close relationship with the oxytrichids (Chen et al. 2017). Therefore, the evolutionary relationships of *Parabistichella, Orthoamphisiella,* and *Tachysoma,* and the systematic position of *Parabistichella* remain unresolved.

Based on the findings presented here, *U. magnigranulosus* may be the closest relative of *Parabistichella*. *Uroleptoides magnigranulosus* has cortical granules similar to those of *P. variabilis.* However, *U. magnigranulosus* differs from the latter in possessing a shorter amphisiellid median cirral row (called the frontoventral row in *Parabistichella*) and in the absence of a second frontoventral row (Berger 2008; Foissner et al. 2002).

The genera *Lamtostyla* and *Bistichella* cluster within the same clade as *Parabistichella*, which is consistent with previous findings based on SSU rDNA sequence data (Dong et al. 2016; Fan et al. 2014; Jiang et al. 2013; Luo et al. 2017). The genus *Lamtostyla* has been treated as a member of the family Amphisiellidae, but the systematic placement of *Bistichella* remains unresolved (Dong et al. 2016; Fan et al. 2014; Jiang et al. 2013; Luo et al. 2017). Both genera, however, can be easily separated from *Parabistichella*: *Lamtostyla* is characterized by its short amphisiellid median cirral row, which usually terminates in the anterior half of the body (vs. near transverse cirri in *Parabistichella*), and *Bistichella* lacks transverse cirri (vs. present in *Parabistichella*).

ACKNOWLEDGMENTS

This work was supported the National Nature Science Foundation of China (project numbers: 41876151 to XP Fan, 31772431 to LF Li, 31672249 to B Ni) and Nature Science Foundation of Shandong Province (project number: ZR2019QD015 to XM Chen).

LITERATURE CITED

Bannister, L. H. 1972. The structure of trichocysts in *Paramecium caudatum*. *J. Cell Sci.*, 11:899–929.

Bardele, C. F. 1981. Functional and phylogenetic aspects of the ciliary membrane: a comparative freeze-fracture study. *Biosystems*, 14:403–421.

Berger, H. 1999. Mongraph of the Oxytrichidae (Ciliophore, Hypotrichia). *Monogr. Biol.*, 78:1–1080.

Berger, H. 2006. Monograph of the Urostyloidea (Ciliophora, Hypotricha). *Monogr. Biol.*, 85:1–1304.

Berger, H. 2008. Monograph of the Amphisiellidae and Trachelostylidae (Ciliophora, Hypotricha). *Monogr. Biol.*, 88:1–737.

Berger, H. 2011. Monograph of the Gonostomatidae and Kahliellidae (Ciliophora, Hypotricha). *Monogr. Biol.*, 90:1–741.

Berger, H. & Foissner, W. 1987. Morphology and biometry of some soil hypotrichs (Protozoa: Ciliophora). *Zool. Jb. Syst.*, 114:193–239.

Bradbury, P., Deroux, G. & Campillo, A. 1987. The feeding apparatus of a chitinivorous ciliate. *Tissue Cell*, 19:351–363.

Calvo, P., Torres, A., Fedriani, C., Rios, R. & Silva, J. P. 1986. Ultrastructure chez *Histriculus similis* (Cilié Hypotriche). *Acta Protozool.*, 25:23–32.

Carey, P. G. & Tatchell, E. C. 1983. A revision of the genus *Epiclintes* (Ciliophora: Hypotrichida) including a redescription of *Epiclintes felis* comb. n. *Bull. Br. Mus. nat. Hist. (Zool.)*, 45:41–54.

Chen, L., Zhao, X., Hamed, A. E. S., Huang, J. & Clamp, J. C. 2017. Systematic studies on the hypotrich ciliate, *Tachysoma pellionellum* (Müller, 1773) Borror, 1972 (Protozoa, Ciliophora) based on integrative analyses: morphology, morphogenesis and molecular phylogeny. *Acta Protozool.*, 56:221–233.

Dallai, R. & Luporini, P. 1981. Membrane specializations in the ciliate *Euplotes crassus* at the site of interaction of the ampules with the plasma membrane. *Eur. J. Cell Biol.*, 23:280–285.

Dong, J., Li, L., Fan, X., Ma, H. & Warren, A. 2020. Two *Urosoma* species (Ciliophora, Hypotrichia): a multidisciplinary approach provides new insights into their ultrastructure and taxonomy. *Eur. J. Protistol.*, 72:125661.

Dong, J., Lu, X., Shao, C., Huang, J. & Al-Rasheid, K. A. 2016. Morphology, morphogenesis and molecular phylogeny of a novel saline soil ciliate, *Lamtostyla salina* n. sp. (Ciliophora, Hypotricha). *Eur. J. Protistol.*, 56:219–231.

Eigner, P. & Foissner, W. 1991. *Orthoamphisiella stramenticola* nov. gen., nov. spec., a new hypotrichous ciliate (Ciliophora: Hypotrichida) occurring in walnut leaf litter. *Acta Protozool.*, 30:129–133.

Eisler, K. & Peck, R. K. 1998. Ultrastructural analysis of the cortical modifications during trichocyst secretory granule docking in the ciliate *Pseudomicrothorax dubius*. *Eur. J. Protistol.*, 34:39–50.

Fan, Y., Hu, X., Gao, F., Al-Farraj, S. A. & Al-Rasheid, K. A. 2014. Morphology, ontogenetic features and SSU rRNA gene-based phylogeny of a soil ciliate, *Bistichella cystiformans* spec. nov. (Protista, Ciliophora, Stichotrichia). *Int. J. Syst. Evol. Microbiol.*, 64:4049–4060.

Fauré-Fremiet, E. & André, J. 1968. Fine structure of *Euplotes eurystomus* (Wrz). *Arch. Anat. Microsc. Morphol. Exp.*, 57:53–78.

Fischer-Defoy, D. & Hausmann, K. 1981. Microtubules, microfilaments, and membranes in phagocytosis: structure and function of the oral apparatus of the ciliate *Climacostomum virens*. *Differentiation*, 20:141–151.

Fleury, A. 1988. The use of correlated ultrastructural and morphogenetic characters in evolutionary taxonomy of hypotrich ciliates. *Biosystems*, 21:309–316.

Foissner, W. 1998. An updated compilation of world soil ciliates (Protozoa, Ciliophora), with ecological notes, new records, and descriptions of new species. *Eur. J. Protistol.*, 34:195–235.

Foissner, W. 2016. Terrestrial and Semiterrestrial Ciliates (Protozoa, Ciliophora) from Venezuela and Galápagos. Denisia. 35.

Foissner, W., Agatha, S. & Berger, H. 2002. Soil Ciliates (Protozoa, Ciliophora) from Namibia (Southwest Africa), with Emphasis on Two Contrasting Environments, the Etosha Region and the Namib Desert. Part I: Text and Line Drawings. Part II: Photographs. Denisia. 5.

Foissner, W. & Al-Rasheid, K. 2006. A unified organization of the stichotrichine oral apparatus, including a description of the buccal seal (Ciliophora: Spirotrichea). *Acta Protozool.*, 45:1–16.

Foissner, W., Müllerb, H. & Agatha, S. 2007. A comparative fine structural and phylogenetic analysis of resting cysts in oligotrich and hypotrich Spirotrichea (Ciliophora). *Eur. J. Protistol.*, 43:295–314.

Foissner, W. & Stoeck, T. 2011. *Cotterillia bromelicola* nov. gen., nov. spec., a gonostomatid ciliate (Ciliophora, Hypotricha) from tank bromeliads (Bromeliaceae) with de novo originating dorsal kineties. *Eur. J. Protistol.*, 47:29–50.

Gao, F., Warren, A., Zhang, Q., Gong, J., Miao, M., Sun, P., Xu, D., Huang, J., Yi, Z. & Song, W. 2016. The all-data-based evolutionary hypothesis of ciliated protists with a revised classification of the phylum Ciliophora (Eukaryota, Alveolata). *Sci. Rep.*, 6:24874.

Gong, Z. W., Fan, X. P., Ma, R. & Ni, B. 2018. Ultrastructure of vegetative cells and resting cysts, and live observations of the encystation and excystation processes in *Diophrys oligothrix* Borror, 1965 (Protista, Ciliophora). *J. Morphol.*, 279:1397–1407.

Görtz, H. D. 1982. Discharge of cortical ampules in *Euplotes aediculatus* Pierson, 1943 (Ciliophora, Hypotrichida). *Arch. Protistenk.*, 125:31–40.

Grim, J. N. 1972. Fine structure of the surface and infraciliature of *Gastrostyla steinii*. *J. Eukaryot. Microbiol.*, 19:113–126.

Grimes, G. W. 1972. Cortical structure in nondividing and cortical morphogenesis in dividing *Oxytricha fallax*. *J. Protozool.*, 19:428–445.

Gu, F., Chen, L., Ni, B. & Zhang, X. 2002. A comparative study on the electron microscopic enzymo-cytochemistry of *Paramecium bursaria* from light and dark cultures. *Eur. J. Protistol.*, 38:267–278.

Gu, F. & Ni, B. 1993. The exploration of preparing protozoan specimen for scanning electron microscopy. *J. Chin. Electron Microsc. Soc.*, 12:525–529.

Gu, F. & Ni, B. 1995. An ultrastructural study on resting cyst of *Euplotes encysticus*. *Acta Biol. Exp. Sin.*, 28:163–171.

Hausmann, K. 1978. Extrusive organelles in protists. *Int. Rev. Cytol.*, 52:197–276.

Hemberger, H. 1985. Neue gattungen und arten hypotricher ciliaten. *Arch. Protistenk.*, 130:397–417.

Huang, J., Luo, X., Bourland, W. A., Gao, F. & Gao, S. 2016. Multigene-based phylogeny of the ciliate families Amphisiellidae and Trachelostylidae (Protozoa: Ciliophora: Hypotrichia). *Mol. Phylogenet. Evol.*, 101:101–110.

Jerka-Dziadosz, M. 1982. Ultrastructural study on development of the hypotrich ciliate *Paraurostyla weissei*. IV. Morphogenesis of dorsal bristles and caudal cirri. *Protistologica*, 18:237–251.

Jiang, J., Huang, J., Li, L., Shao, C., Al-Rasheid, K. A., Al-Farraj, S. A. & Chen, Z. 2013. Morphology, ontogeny, and molecular phylogeny of two novel bakuellid-like hypotrichs (Ciliophora: Hypotrichia), with establishment of two new genera. *Eur. J. Protistol.*, 49:78–92.

Kloetzel, J. A. 1974. Feeding in ciliated protozoa: i. Pharyngeal disks in *Euplotes*: a source of membrane for food vacuole formation. *J. Cell Sci.*, 15:379–401.

Kumar, S., Stecher, G., Li, M., Knyaz, C. & Tamura, K. 2018. MEGA X: Molecular evolutionary genetics analysis across computing platforms. *Mol. Biol. Evol.*, 35:1547–1549.

Landan, G. & Dan, G. 2008. Local reliability measures from sets of co-optimal multiple sequence alignments. *Pac. Symp. Biocomput.*, 13:15–24.

Lenzi, P. & Rosati, G. 1993. Ultrastructural study of *Euplotidium itoi* (Ciliata Hypotrichida). *Eur. J. Protistol.*, 29:453–461.

Luo, X., Gao, F., Yi, Z., Pan, Y., Al-Farraj, S. A. & Warren, A. 2017. Taxonomy and molecular phylogeny of two new brackish hypotrichous ciliates, with the establishment of a new genus (Ciliophora, Spirotrichea). *Zool. J. Linn. Soc.*, 179:475–491.

Luo, X., Huang, J. A., Li, L., Song, W. & Bourland, W. A. 2019. Phylogeny of the ciliate family Psilotrichidae (Protista, Ciliophora), a curious and poorly-known taxon, with notes on two algae-bearing psilotrichids from Guam, USA. *BMC Evol. Biol.*, 19:125.

Lynn, D. 2008. The ciliated protozoa: characterization, classification, and guide to the literature. 3rd edition. Springer, Dordrecht.

Medlin, L., Elwood, H. J., Stickel, S. & Sogin, M. L. 1988. The characterization of enzymatically amplified eukaryotic 16S-like rRNA-coding regions. *Gene*, 71:491–499.

Moon, J. H., Kim, J. H., Quintela-Alonso, P. & Jung, J. H. 2019. Morphology, morphogenesis, and molecular phylogeny of *Neobakuella aenigmatica* n. sp. (Ciliophora, Spirotrichea, Bakuellidae). *J. Eukaryot. Microbiol.*, 1–12.

Morelli, A., Giambelluca, A., Lenzi, P., Rosati, G. & Verni, F. 1996. Ultrastructural features of the peculiar filter-feeding hypotrich ciliate *Uronychia transfuga*. *Micron*, 27:399–406.

Nylander, J. A. A. 2004. MrModeltest V2. Program Distributed by the Author. Evolutionary Biology Centre, Uppsala University.

Paiva, T. D. S., Borges, B. D. N., Silva-Neto, I. D. & Harada, M. L. 2012. Morphology and 18S rDNA phylogeny of *Hemicycliostyla sphagni* (Ciliophora, Hypotricha) from Brazil with redefinition of the genus *Hemicycliostyla*. *Int. J. Syst. Evol. Microbiol.*, 62:229–241.

Pan, X., Bourland, W. A. & Song, W. 2013. Protargol synthesis: an in-house protocol. *J. Eukaryot. Microbiol.*, 60:609–614.

Park, K., Chae, N., Jung, J. H., Min, G. S., Kim, S. & Berger, H. 2017. Redescription of *Keronopsis helluo* Penard, 1922 from Antarctica and *Paraholosticha pannonica* Gellért and Tamás, 1959 from Alaska (Ciliophora, Hypotricha). *Eur. J. Protistol.*, 60:102–118.

Park, K., Jung, J. & Min, G. 2013. Morphology, morphogenesis, and molecular phylogeny of *Anteholosticha multicirrata* n. sp. (Ciliophora, Spirotrichea) with a note on morphogenesis of *A. pulchra* (Kahl, 1932) Berger, 2003. *J. Eukaryot. Microbiol.*, 60:564–577.

de Puytorac, P., Grain, J., de Santa, R. & Rosa, M. 1976. A propos de l'ultrastructure corticale du cilié hypotriche *Stylonychia mytilus* Ehrbg., 1838: les caracteristiques du cortex buccal adoral et paroral des Polyhymenophora Jankowski, 1967. *Trans. Am. Microsc. Soc.*, 95:327–345.

Ronquist, F. & Huelsenbeck, J. P. 2003. MrBayes 3: Bayesian phylogenetic inference under mixed models. *Bioinformatics*, 19:1572–1574.

Rosati, G. & Modeo, L. 2003. Extrusomes in ciliates: diversification, distribution, and phylogenetic implications. *J. Eukaryot. Microbiol.*, 50:383–402.

Rosati, G., Verni, F., Bracchi, P. & Dini, F. 1987. An ultrastructural analysis of the ciliated protozoon *Aspidisca* sp. *Trans. Am. Microsc. Soc.*, 106:31–52.

Roth, L. 1957. An electron microscope study of the cytology of the protozoan *Euplotes patella*. *J. Biophys. Biochem. Cytol.*, 3:985–1000.

Schmidt, S. L., Bernhard, D., Schlegel, M. & Foissner, W. 2007. Phylogeny of the Stichotrichia (Ciliophora; Spirotrichea) reconstructed with nuclear small subunit rRNA gene sequences: discrepancies and accordances with morphological data. *J. Eukaryot. Microbiol.*, 54:201–209.

Sela, I., Ashkenazy, H., Katoh, K. & Pupko, T. 2015. GUIDANCE2: accurate detection of unreliable alignment regions accounting for the uncertainty of multiple parameters. *Nucleic Acids Res.*, 43:W7–W14.

Shigenaka, Y., Watanabe, K. & Kaneda, M. 1973. Effects of glutaraldehyde and osmium tetroxide on hypotrichous ciliates, and determination of the most satisfactory fixation methods for electron microscopy. *J. Protozool.*, 20:414–420.

Song, W. B. & Shao, C. 2017. Ontogenetic Patterns of Hypotrich Ciliates. Science Press, Beijing (in Chinese).

Stamatakis, A., Hoover, P. & Rougemont, J. 2008. A rapid bootstrap algorithm for the RAxML Web servers. *Syst. Biol.*, 57:758–771.

Sui, S., Chen, Y., Qiu, Z. & Shi, X. 2001. Structure of oral apparatus in *Stylonychia mytilus*. *Acta Zool. Sin.*, 47:436–441.

Tang, W. J., Fan, X. P., Bing, N. I. & Fu-Kang, G. U. 2016. Study on extrusomes of the hypotrichous ciliate *Oxytricha granulifera* (Ciliophora: Hypotrichida). *J. Biol.*, 33:38–42.

Vd'ačný, P. & Foissner, W. 2017. A huge diversity of metopids (Ciliophora, Armophorea) in soil from the Murray River floodplain, Australia. I. Description of five new species and redescription of *Metopus setosus* Kahl, 1927. *Eur. J. Protistol.*, 58:35–76.

Verni, F. & Gualtieri, P. 1997. Feeding behaviour in ciliated protists. *Micron*, 28:487–504.

Wang, J., Li, J., Qi, S., Warren, A. & Shao, C. 2019. Morphogenesis and molecular phylogeny of a soil ciliate *Uroleptoides longiseries* (Foissner, Agatha and Berger, 2002) Berger 2008 (Ciliophora, Hypotrichia). *J. Eukaryot. Microbiol.*, 66:334–342.

Wessenberg, H. & Antipa, G. 1970. Capture and ingestion of *Paramecium* by *Didinium nasutum*. *J. Eukaryot. Microbiol.*, 17:250–270.

Wicklow, B. J. 1983. Ultrastructure and cortical morphogenesis in the euplotine hypotrich *Certesia quadrinucleata* Fabre-Domergue, 1885 (Ciliophora, Protozoa). *J. Eukaryot. Microbiol.*, 30:256–266.

Wilbert, N. 1975. Eine verbesserte technik der protargolimprägnation für ciliaten. *Mikrokosmos*, 64:171–179.

Wirnsberger, E. & Hausmann, K. 1988. Fine structure of *Pseudokeronopsis carnea* (Ciliophora, Hypotrichida). *J. Eukaryot. Microbiol.*, 35:182–189.

Wirnsberger-Aescht, E., Foissner, W. & Foissner, I. 1989. Morphogenesis and ultrastructure of the soil ciliate *Engelmanniella mobilis* (Ciliophora, Hypotrichida). *Eur. J. Protistol.*, 24:354–368.

Xu, Y., Gao, F. & Fan, X. 2018. Reconsideration of the systematics of Peniculida (Protista, Ciliophora) based on SSU rRNA gene sequences and new morphological features of *Marituja* and *Disematostoma*. *Hydrobiologia*, 806:313–331.

Zhang, J., Ni, B., Sheng, C. & Gu, F. K. 2007. Observations on the ultrastructure of mucocyst in *Urostyla grandis*. *Fudan Univ. J. Med. Sci.*, 46:972–975.

Zhang, J., Sheng, C., Tang, L., Ni, B. & Gu, F. 2011. The ultrastructure of the extrusomes in *Pseudourostyla cristata*, a hypotrichous ciliated protozoan. *Protoplasma*, 248:475–481.

Zhang, X., Yang, L., Wang, Y., Ni, B., Al-Farraj, S. A., Fan, X. & Gu, F. 2014. Observations on the ultrastructure of extrusomes in the hypotrichous ciliate *Architricha indica* (Protist, Ciliophora). *Anim. Cells Syst.*, 18:83–92.

Zhang, X., Zhai, Y., Ni, B. & Gu, F. 2012. Observations on the ultrastructure of extrusomes in *Anteholosticha monilata* (Ciliophora: Hypotrichida). *Chin. J. Cell Biol.*, 34:174–178.

Zhou, Y., Wang, Z., Zhang, J. & Gu, F. 2011. Ultrastructure of extrusomes in hypotrichous ciliate *Pseudourostyla nova*. *Chin. J. Oceanol. Limnol.*, 29:103–108.